



Polymer-Gel Radiation Dosimetry of Laser-Based Relativistic Electron Sources for Biomedical Applications: First Qualitative Results and Experimental Challenges

OPEN ACCESS

Edited by:

Antonino Picciotto,
Bruno Kessler Foundation (FBK), Italy

Reviewed by:

Mauro Valente,
CCT CONICET Córdoba, Argentina
Andreas Berg,
Medical University of Vienna, Austria

*Correspondence:

Michael Tatarakis
mictat@hmuu.gr

Specialty section:

This article was submitted to
Interdisciplinary Physics,
a section of the journal
Frontiers in Physics

Received: 18 June 2021

Accepted: 14 March 2022

Published: 07 April 2022

Citation:

Fitis I, Grigoriadis A, Tazes I, Petrakis S, Andrianaki G, Dimitriou V, Bakarezos E, Benis EP, Tsiapa I, Boursianis T, Kalaitzakis G, Bontzos G, Liakopoulos DA, Pappas E, Detorakis ET, Clark EL, Maris TG, Papadogiannis NA and Tatarakis M (2022) Polymer-Gel Radiation Dosimetry of Laser-Based Relativistic Electron Sources for Biomedical Applications: First Qualitative Results and Experimental Challenges. *Front. Phys.* 10:727511. doi: 10.3389/fphy.2022.727511

Ioannis Fitis^{1,2}, Anastasios Grigoriadis^{1,3}, Ioannis Tazes^{1,2}, Stelios Petrakis^{1,3}, Georgia Andrianaki^{1,4}, Vasilios Dimitriou^{1,5}, Efthimios Bakarezos^{1,5}, Emmanouil P. Benis^{1,3}, Irimi Tsiapa⁶, Themistoklis Boursianis⁶, Georgios Kalaitzakis⁶, Georgios Bontzos^{7,8}, Dimitrios A. Liakopoulos^{7,8}, Evangelos Pappas⁹, Efstathios T. Detorakis^{7,8}, Eugene L. Clark¹, Thomas G. Maris⁶, Nektarios A. Papadogiannis^{1,5} and Michael Tatarakis^{1,2*}

¹Institute of Plasma Physics and Lasers, Hellenic Mediterranean University Research Centre, Rethymno, Greece, ²Department of Electronic Engineering, Hellenic Mediterranean University, Chania, Greece, ³Department of Physics, University of Ioannina, Ioannina, Greece, ⁴School of Production Engineering and Management, Technical University of Crete, Chania, Greece, ⁵Department of Music Technology and Acoustics, Hellenic Mediterranean University, Rethymno, Greece, ⁶Department of Medical Physics, School of Medicine, University of Crete, Heraklion, Greece, ⁷Department of Ophthalmology, University Hospital of Heraklion, Heraklion, Greece, ⁸School of Medicine, University of Crete, Heraklion, Greece, ⁹Department of Biomedical Sciences, Radiology and Radiotherapy Sector, University of West Attica, Athens, Greece

The generation of laser based relativistic electron sources involves impressive basic science as well as innovative applications. This study reports first novel qualitative results on polymer-gel radiation dosimetry of ultrafast laser-based relativistic electron beams. The fabricated polymer-gels are irradiated by the ultra-high dose rate (FLASH) laser-generated electron beams and then are analysed using magnetic resonance imaging. The reading of the irradiated dosimeters is performed using a clinical 1.5 T Magnetic Resonance Imaging system. Three-dimensional colour parametric T2 maps are then constructed from the original PD-T2 weighted images obtained from the clinical MRI scanner. For comparison, the gels are also irradiated with standard electron beams of various energies utilizing a radiotherapy clinical linear accelerator system. For the calibration measurements of the gel dosimetry method, special calibrated dosimetric films are also implemented. The preliminary results demonstrate the potential of polymer gel dosimetry for 3D-dose-distribution of FLASH type irradiation of laser generated electron beams. Furthermore, they illustrate potential issues related to the polymer gel based dosimetry in challenging irradiation arrangements, such as the oxygen sensitivity and necessity for oxygen impermeable container material.

Keywords: phantom polymer gel, laser acceleration, radiation dosimetry, biomedical application, FLASH radiation

1 INTRODUCTION

High-intensity lasers had a strong impact on the evolution of a wide range of fields in science and technology. The implementation of Chirped Pulsed Amplification (CPA) [1] has boosted the development of laser systems capable of producing short pulses with extremely high peak-power, which, when focused, can provide intensities currently approaching 10^{23} W/cm². During intense laser-matter interactions exceeding 10^{18} W/cm² the ponderomotive potential energy of plasma electrons quivering in the field of the laser, approaches or exceeds the rest energy of electron, thus enabling the capability for the investigation of new phenomena in the high-energy physics and the development of important emerging applications. The extreme fields during the intense laser-matter interaction can drive secondary sources of high energy photons and particles emission [2–11]. By combining the appropriate target (i.e., thick/thin solid targets, gas jets, clusters, etc.) and laser interaction conditions, it is possible to control the generation of X-ray radiation as well as of energetic particles (ions/protons and electrons).

Accelerated energetic particles such as electrons, protons and ions have important applications in bio-medicine, as also in material science, chemistry, agro-alimentary, nuclear physics and many other areas. Conventionally, they are produced by large synchrotrons, LINear ACcelerator (LINAC) or radioactive nuclei. The ability to create such sources by lasers offers many advantages [12]. Various mechanisms of laser-driven electron and proton/ions accelerators have been suggested and utilized. One of the well-established reliable methods for proton/ion acceleration is the so-called Target Normal Sheath Acceleration (TNSA) for laser interaction with solid targets [13]. For electron beams, the state of the art is the Laser Wake Field Acceleration (LWFA) in the bubble regime [14, 15] that achieves electron energies up to GeVs [16], the energy range of large-scale synchrotron facilities. Since the value of the laser electric field of ultra-intense laser pulses is more than 10^4 times greater than the electric field generated in conventional schemes, the length required to generate these sources is orders of magnitude smaller (even less than a millimetre) than that required in conventional sources. Additionally, the brightness and the ultrafast pulse duration of these beams make them unique and distinctive from other conventional sources, opening new fields in radiobiology research [17–19].

For the characterization of the particle beams, various diagnostics have been developed or adjusted according to the requirements of the applications and to the specific characteristics of the beams. The diagnostics for total and spatially resolved charge measurements of laser-driven beams have generally a different designation approach compared to that used in the conventional accelerators [20, 21]. The ultrafast pulsed nature of these beams, where high bunch charged particles are emitted in very short pulses, produces high current peaks. Also, the hostile environment of the laser target interaction area must be considered for measurements close to the source. Since electronics can interfere with the strong electromagnetic pulses (EMPs) produced, the use of passive diagnostics often becomes

valuable [22]. Post-processing particle diagnostics such as the radiochromic film (RCF), CR-39 nuclear tracker and image plates (IP), as well as scintillating screens (LANEX) for on-line beam characterization, are insensitive to EMPs and are widely used in laser-driven beam diagnostics, while sophisticated analysis is applied to extract valuable information of the beam characteristics [23].

In this work, polymer gels based on the VIPET formulation were used for the characterization of electron beams. The electron beams were generated by the interaction of high intensity laser pulses with solid targets at the Institute of Plasma Physics and Laser (IPPL¹) of the Hellenic Mediterranean University (HMU). The fabrication of VIPET gel solutions was adapted according to the needs of the specific electron dosimetry challenges. It is extremely challenging to use polymer gel dosimeters in either research or clinical environments for highly accurate absolute dosimetry [24]. However, the dose response, in most types of polymer gels, is linear up to a polymer gel specific saturation regime and thus precise 3D-relative dose data can in principle be obtained if reproducible readout-methods are used. The preferred measurement tools in dosimetry are 0D/1D dosimeters (such as ionization chambers) for absolute dose measurements with high accuracy, 2D dosimeters (such as films) for 2D relative and/or absolute dosimetry, and 3D-polymer gels for 3D-relative dosimetry. All relative dose measurements can be normalized to a trusted and high accurate 0D/1D ionization chamber measurement, or a calibrated 2D film dosimeter. For all these reasons, over the last decade polymer gel dosimetry has gained a major role in three clinical dosimetry applications: 1) single-isocentric stereotactic radiosurgery (SRS) for multiple metastases [25], 2) proton therapy [26] and 3) Magnetic Resonance Linear Accelerator (MR-LINAC) based radiotherapy [27]. All these radiotherapy (RT) techniques are of increasing importance and are rapidly spreading worldwide. A new area of application of polymer gels might arise for basic dosimetric experiments with highly energetic beams of various origins and literally unknown characteristics, such as in FLASH irradiation techniques. The combination of the unique characteristics of the polymer gels, the advancements in radiation oncology, and the rising challenges that affect the safety of the treatment in general, might make polymer gel 3D dosimetry an integral part of the clinical practice of advanced RT applications or RT research endeavours [28].

The FLASH dose deposited into the gel by the short electron bunches generated in these experiments, is analysed by a clinical Magnetic Resonance Imaging (MRI) system. Processing of the measured characteristic parameter T2 of the irradiated gel provides a 3-D map of the gel polymerization ratio which is correlated to the deposited dose. By the selective adjustment of the composition of the gel, the sensitivity or the dynamic range of the dosimetry can be controlled, in order to be adapted to the specific characteristics of the source. For the calibration of the gel dosimeters, a radiotherapy clinical LINAC source is utilized. In addition, measurements using the conventional method of

¹www.ippl.hmu.gr.

radiochromic films are also implemented to provide evidence for the results. The unique feature of the inherent three-dimensional character of the gel dosimetry method is demonstrated here for a laser generated electron beam. Thus, the advantage over 2D-methods as e.g. planar film dosimetry is confirmed also for this application. The preliminary results presented here shed light on the various aspects to be considered for the useful application of 3D polymer gel dosimetry. However, our results outline some of the problems and experimental difficulties in applying polymer gel dosimetry as a tissue equivalent 3D-dosimeter for novel irradiation concepts and extraordinary field applications.

2 MATERIALS AND METHODS

2.1 The Laser-Driven Accelerator

In this paper we describe a VIPET polymer gel container set-up that is adapted to the specific electron dosimetry challenges of laser generated MeV electron beams. In particular, it is adapted to characterize the electron beams generated when the ZEUS 45 TW laser system of IPPL-HMU, interacts with thin aluminium foil targets [29]. The laser system, developed by Amplitude Technologies, is capable of producing laser pulses of energy over 1 J and duration less than 25 fs. The output laser beam is delivered under vacuum to the experimental chamber where the interaction with the target takes place. The experimental layout can be seen in **Figure 1A**, while in **Figure 1B** an image of the optical setup inside the experimental chamber is presented. The main interaction beam is 55 mm in diameter and it is steered in the vacuum chamber by using a pair of dielectric mirrors guided onto an $f/2$ off-axis parabola. The focal spot is optimized by fine adjustment of the parabolic mirror while it is monitored by a beam profile camera. The focal spot in these experiments has a diameter at FWHM (Full Width Half Maximum) better than $3\ \mu\text{m}$ (**Figure 1C**), so an intensity up to $6 \times 10^{20}\ \text{W}/\text{cm}^2$ on target is achieved. The target used in these experiments is a $30\ \mu\text{m}$ thick aluminium foil. The laser beam is focused onto the target at an angle of 45° to the target normal. Retro-reflection imaging of the laser spot on target at low energy is used to optimize the target position prior to each shot. In addition, the laser-plasma interaction is monitored in shot-to-shot basis via laser probe imaging diagnostics utilizing the 10 mJ, 25 fs probe laser pulses delivered by the ZEUS laser system. A re-entrant tube, with a $150\ \mu\text{m}$ thick plastic viewport for separation from vacuum chamber, is used to deliver under atmospheric pressure, the vial with the gel close to the particles source. The entrance edge of the vial has a distance of 4 cm from the rear of the target (**Figure 1A**). The interaction of the high intensity laser pulses with the solid target, in principle follows the Target Normal Sheath Acceleration (TNSA) mechanism [13]. The mechanism strongly depends on parameters such as the material, the thickness of the target, the laser and the focal conditions. For the experiments in this work, the prepulse of the laser beam induces preplasma formation on the target front that results in low energy proton emission [29]. Due to proper filtering of these protons the dose deposited in gels is attributed

mainly to the dominating emission of electrons and to a potentially small contribution of x-rays emitted from the target area.

2.2 Conventional Diagnostics

2.2.1 CR39 Nuclear Track Detectors

In order to measure the emission of protons from the laser-driven secondary radiation source and exclude their contribution to the dose measurements, the well-known CR39 solid state nuclear track detector is used. As a proton passes through a material, most of its energy is lost at a certain depth giving the characteristic *Bragg peak*. The highly localized energy deposition of protons or ions can cause damages on the CR39 by breaking bonds in the material structure. For electrons on the other hand, the energy loss as a function of distance is almost constant and therefore makes CR39 relatively insensitive to electron damage. If the proton or ion has an energy which results in stopping close to the surface of the CR39, then the damage will be generated in this region. To reveal these damages, the CR39 is etched by soaking in concentrated sodium hydroxide (20% by weight NaOH) solution for 3 h at 90°C . The material is slowly dissolved away from the surface, but at the damaged areas the CR39 is etched to a greater extent and a pit or cavity is formed. CR39 has a characteristic damage threshold and thus a minimum amount of energy is required to induce damage. It is sensitive to ions and protons with energies higher than $100\ \text{keV}/\text{nucleon}$ and has the unique characteristic that one pit (cavity) is etched by each proton or ion that has stopped close to the surface.

To determine the maximum energy of the proton beam, an aluminium filter array consisting of eight (8) sectors of different thickness of aluminium is placed in front of a single piece of CR39 and aligned with the rear target normal of the target at a distance of 2 cm, as shown in **Figure 2A**. Only protons with sufficient energy can pass through each sector. Using knowledge of the range of the protons in aluminium as a function of their kinetic energy, the maximum proton energy is determined [29]. The propagation range of protons in aluminium and CR39 as a function of their energy is illustrated in **Figure 2B**, where the data is derived using the SRIM² software.

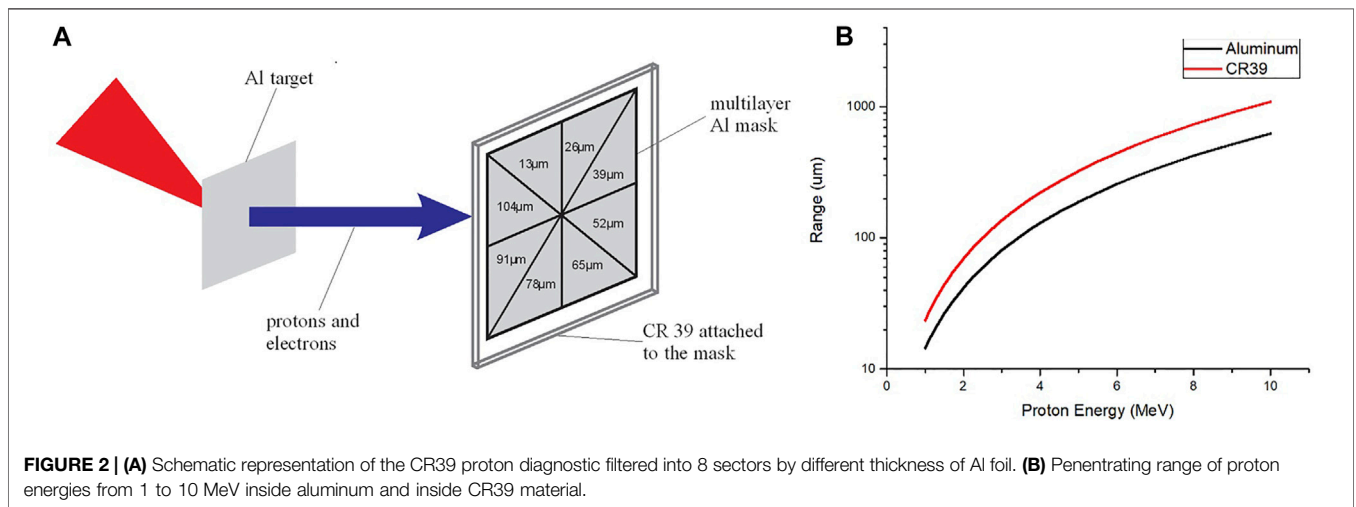
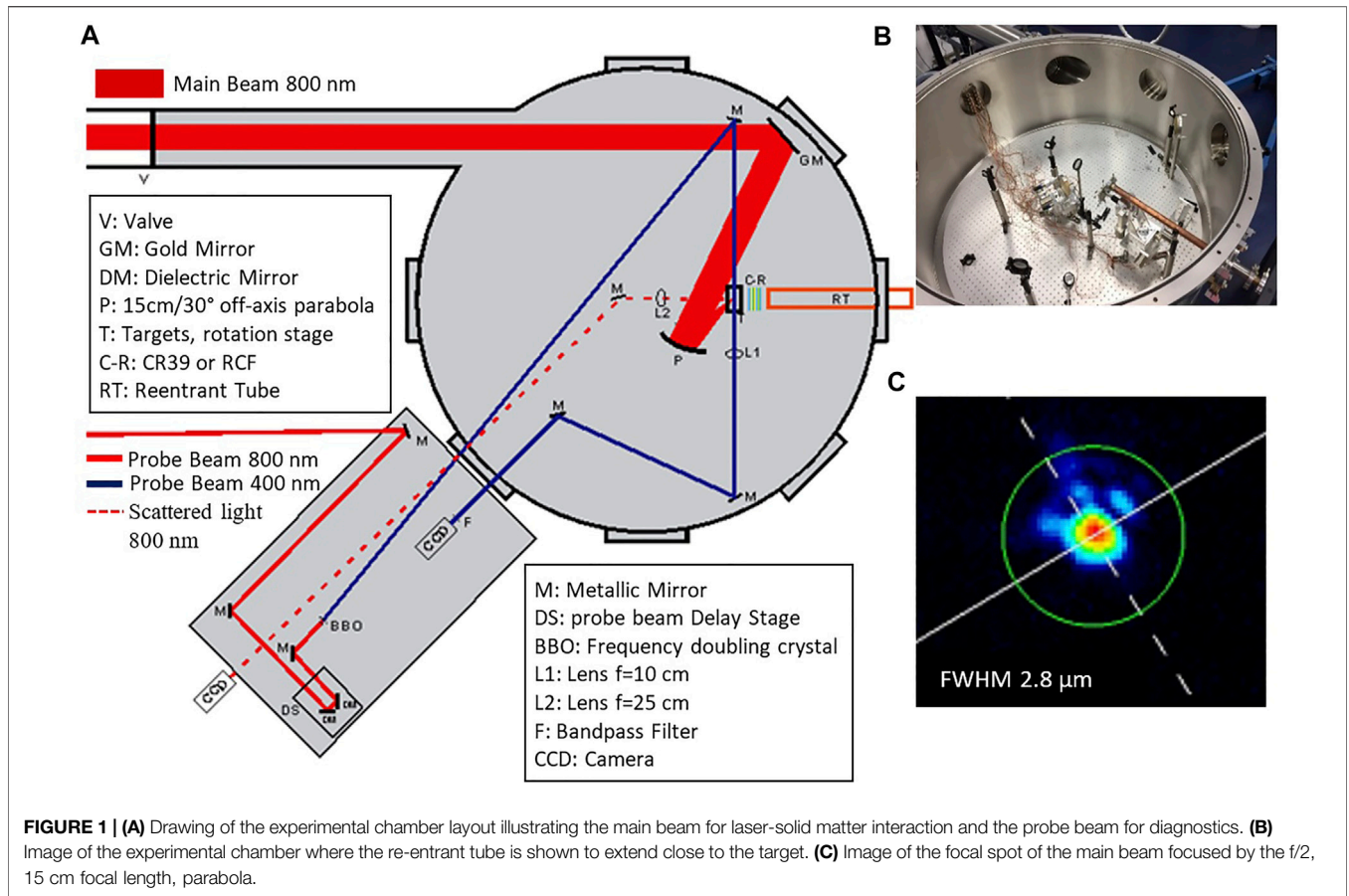
2.2.2 Radiochromic Film

Radiochromic film (RCF) is used in these experiments for radiation dose measurements. When exposed to ionizing radiation, the active layer of the film undergoes a colour change. The optical density (OD) of the film increases as a function of the radiation dose. The commercially available radiochromic film Gafchromic EBT3, calibrated by RTsafe company³, is used. The EBT3 consists of a $28\ \mu\text{m}$ thick active layer between two $125\ \mu\text{m}$ thick polyester substrates [30]. For film calibration a ^{60}Co monoenergetic beam of known dose rate is utilized.

The RCFs are used in a stack to record the dose deposition degradation, as a function of the ionising radiation energy. The

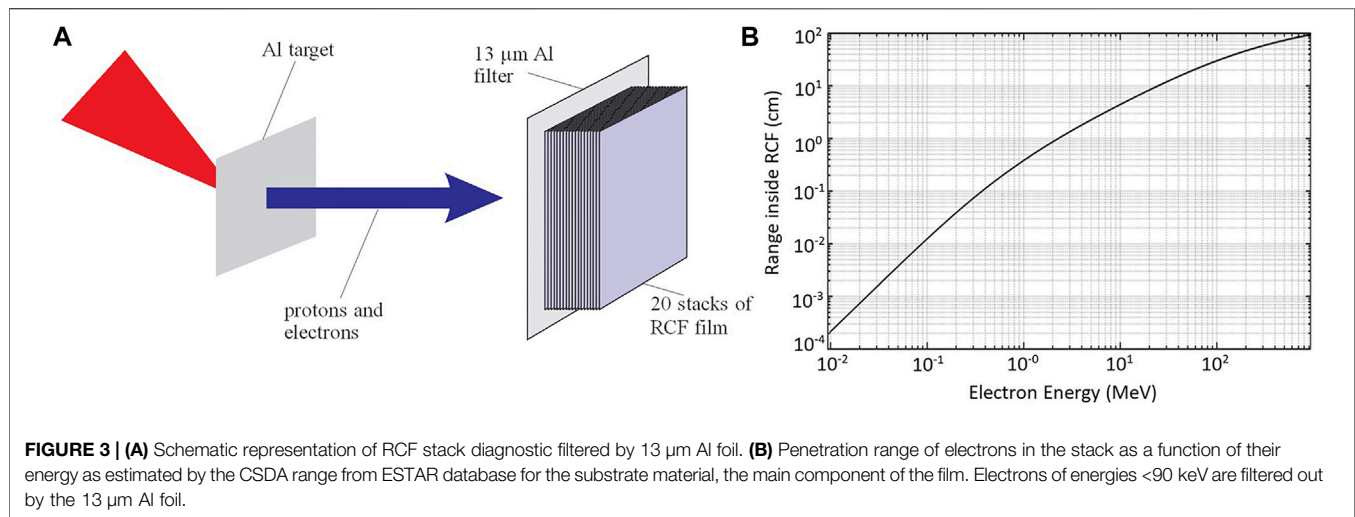
²www.srim.org.

³www.rt-safe.com.



more energetic the particle, the more it penetrates into the stack. A 13 μm Al foil (**Figure 3A**) covers the RCF stack to block the laser radiation affecting the RCF. In these experiments, the dose measured in the films is not attributed to the protons because their energy range, as measured by the CR39, is not sufficient to pass the first layer of RCF. By interleaving a CR39 after the first

RCF of the stack, the absence of any signal recorded on CR39 indicates that in the dose deposited on RCFs stack there is no protons contribution. The photon emission during the laser interaction with the thin low-Z target originates mainly from bremsstrahlung radiation and amounts to about 1% of total emission of ionizing radiation which is dominated by the



electrons [31]. Provided the comparable response of the EBT3 film in electrons and photons irradiation [32], we deduce that the RCF signal is mainly due to electrons. From the dose measurement by the RCFs stack and the stopping power of electrons in the films the electron energy spectrum is evaluated [29, 33]. In **Figure 3B** the Continuous Slowing Down Approximation (CSDA) range of electrons in the film's substrate material by NIST ESTAR database⁴ allows for an estimation of the energy range from the penetration depth in stack.

2.3 Polymeric Gel Diagnostics

Polymer gel dosimeters are chemical dosimeters whose functionality is based on the effect of radiation-induced polymerization [34]. During production, polymer gels are in liquid form and can fill phantoms designed for specific purposes, like a big container or a small vial, of any shape. Following production and after filling a phantom, at room temperature, polymer gels end up at the state of a semi-solid gel. There is a large variety of polymer gels recipes with different toxicities, dose ranges, and sensitivities. Typically, they are composed of 85–90% water, 5–10% gelatine and selected organic monomers and cross-linkers. The gelatine is used as a base for building a robust gel network. Water molecules, organic monomers, and cross-linkers are uniformly distributed within the gel network. By irradiating the polymer gel a radiation-induced polymerization of the monomers and cross-linker takes place. The polymerization is restricted to small volumes usually smaller than the smallest detectable volume element (voxel) in MRI [34] used for reading the extent of polymerization via the MR-contrast parameter T2. The smallest detectable volume with standard human MRI-scanners is approximately $1 \times 1 \times 1 \text{ mm}^3$.

When a polymer gel-filled phantom is irradiated, the spatial distribution of the delivered dose pattern is translated into a spatial distribution of the amount of radiation-induced chemical

changes within the phantom. The level of polymerization depends on the absorbed dose and leads to a local restriction of the molecular motion of the water molecules inside the gel network. In proton (^1H) NMR/MRI theoretical modelling, water molecular motion is related to both nuclear magnetic spin-lattice (T1) and spin-spin (T2) relaxation times according to Bloembergen-Purcell-Pound (BPP) theory [35].

T2 relaxation time is the most sensitive parameter in MR-based polymer-gel dosimetry. It is directly related to the “magnetic molecular vicinity” or “magnetic movement restriction” of the water molecules [35]. T2 shortens with reduced mobility of the embedded water molecules as a consequence of radiation induced polymerization. The relaxation rate R2 actually increases linearly within a large dose range as typically used for radiation therapy. Therefore, by accurately measuring T2 or R2 on a pixel by pixel basis in a 3D pattern utilizing special MRI sequences, the 3D dose distribution can be directly measured. As the 3D dose pattern is trapped within the irradiated polymer gel network, it can be extracted by quantitative MRI (T2 or R2 relaxometry), after a short time of about 1 h and up to few weeks after irradiation.

The radiation-induced polymerization is also leading to an increased optical turbidity, so that, alternatively, simple eye observation and more sophisticated optical scanning of a transparent gel container phantom is possible to determine the 3D-dose information in the gel-filled phantom.

Polymer gels possess some important characteristics and advantages in reference to their utilization as dosimeters. Polymer gels are in general not independent on linear energy transfer (LET) as shown e.g. for proton particle beams in the Bragg peak regime with $\text{LET} > 4.9 \text{ keV}$ [36]. However, as relevant for the investigations here, for low LET irradiations (photons electrons) with clinical energy ranges of 1 up to 20 MeV no LET dependence has been reported [36]. Polymer gels are tissue equivalent (80–85% w/v water), independent of the energy and the LET of the incident particles (photons, electrons, protons, carbon ions etc). They are practically very helpful in overcoming any positioning challenges that are present with standard

⁴<http://physics.nist.gov/Star>.

TABLE 1 | Monomer components and concentrations of VIPET.

VIPET	
Monomer components	Concentration Range
Gelatin	5% w/v
Vinyl	6% w/v
Bis	4% w/v
Distilled water	85% w/v
THPC	7 mM

dosimeters (Films, TLDs) especially for small beam dosimetric data acquisition. They can perform very high 3D spatial resolution dose distribution measurements, of the order of less than 1 mm³ voxel volume limited by the inherent voxel resolution of the reading system (MRI) [34, 37, 38].

Polymer gels dose response might be affected by a variety of parameters like the chemical reagents batch, the production workflow, the time interval between fabrication and irradiation, the time interval between irradiation and MRI scanning/reading, the volume of the gel filled phantom, the internal gel matrix temperature, the oxygen presence within the polymer gel and the NMR/MRI scanner performance [38]. The presented data here are preliminary and the dose rate dependence of the polymer in the investigated FLASH dose rate range has not been investigated yet and is therefore a potential source of dosimetric inaccuracy.

2.3.1 Polymer Gel Synthesis

Polymer gels are present in the literature in different chemical compositions. Their acronyms depend on the type of their gel base, monomer, cross-linker and oxygen scavenger material [37]. The polymer gel dosimeters used here have a gelatine content of 5% weight fraction (wf). This is to be compared with the usual VIPAR gel composition, first presented by Pappas et al (1999) [39]. The modified VIPAR gel composition used in this study, constitutes of a mixture of the monomer N-vinylpyrrolidone (VIPET) in 6% wf, the cross-linker N, N-methylenebisacrylamide (bis) in 4% wf, the gelatine in 5% wf, and double-distilled deionized water in 85% wf. This type of gel is known as VIPET gel [40] and is manufactured in normoxic conditions in the absence of oxygen and in the presence of argon. The monomer components of VIPET gel, as well as their concentrations are presented in **Table 1**.

After each monomer addition, argon gas was added, in order to ensure that the solution is kept under normoxic conditions during fabrication. The use of argon to remove oxygen from the gel solution is necessary to avoid unwanted inhibition of gel polymerization. Moreover, the additional presence of the oxygen scavenger THPC minimizes the unwanted effects of oxygen in the gel polymerization process. The effect of oxygen on the dose sensitivity of the polymer gels has been presented by a number of groups [41–43].

The fabrication procedure is performed as follows: the gelatine is added to the double-distilled deionized water at room temperature (20–25°C) and allowed to dissolve. The solution is then heated to 50°C and once the temperature is stabilized the bis

is added. Heating is achieved through a hot-plate and stirring unit. When the solution becomes transparent and obtains a champagne colour, about 30 min later, the mixture is cooled down to approximately 35°C and then vinyl is added. Once the constituents are completely dissolved after about 5 min, the oxygen scavenger tetrakis (hydroxymethyl)phosphonium chloride (THPC) is added to the solution.

THPC constituent is a clear colourless solution at 80% in water. Care is taken to keep the temperature above 32°C and avoid solidification of the solution. Three minutes after the addition of THPC the gel is transferred to the glass vials of 25 ml total volume (**Figure 4**).

When the final solution is ready, vials filled with the polymer gel material are covered with a “Parafilm” foil to protect the gel surface from atmosphere [40]. After fabrication, all the phantoms (vials) were refrigerated, in the absence of light, to cool down and coagulate at approximately 10°C, 48 h before irradiation. The phantoms (vials) were positioned upright, to minimize the production of air bubbles and were kept sealed with their caps along with the Parafilm foil. The procedure is crucial in order to avoid oxygen contamination of the gel and the use of Parafilm was proven not effective on that. The phantoms gradually adapt to room temperature about half an hour before their irradiation.

2.3.2 Polymer Gel Irradiation

Trial irradiations of polymer gel vial phantoms are performed in the clinical LINAC radiotherapy system of the Radiotherapy department at the University Hospital of Heraklion- PAGNI (INFINITY, 6 MV, ELEKTA, **Figure 5A**) utilizing electron beams at various energies. The following irradiation strategies are used here:

- Electron beam irradiation: A 6 × 6 cm irradiation field is applied using 6 MeV electrons and a standard electron cone, delivering a final dose of 2 and 3 Gys at a depth of 1 cm (this distance starts from the top of the glass vial towards its bottom).

In both irradiations, the dose rate is kept constant at 600 MU/min. This dose rate could be easily achieved in any modern clinical radiotherapy apparatus. These types of irradiations served as reference irradiation beams, in order to visualize and measure via MRI the effect of polymerization on the irradiated gels. The standard electron beam irradiation setup is presented in **Figure 5B**.

For the laser generated electron irradiation the vial with the polymer gel is placed under atmospheric pressure at the end of the re-entrant tube. A 13 μm thick aluminium foil, that blocks the laser radiation from affecting the gel, is placed at the entrance window. The edge of the vial is positioned at a distance of 4 cm from the 30 μm Al target. A number (10 and 30) of successive laser pulses is shot to fresh Al target foil, with a repetition of about 5 min between them. The multiple irradiated gel is taken out from the re-entrant tube and delivered to the MRI analysis.

2.3.3 MRI Reading and Gel Analysis

All polymer gel phantom measurements are performed on a 1.5 T superconducting clinical MR imager (Vision/Sonata hybrid System, Siemens, Erlangen). (Gradient Strength: 40 mT/m, Gradient rise

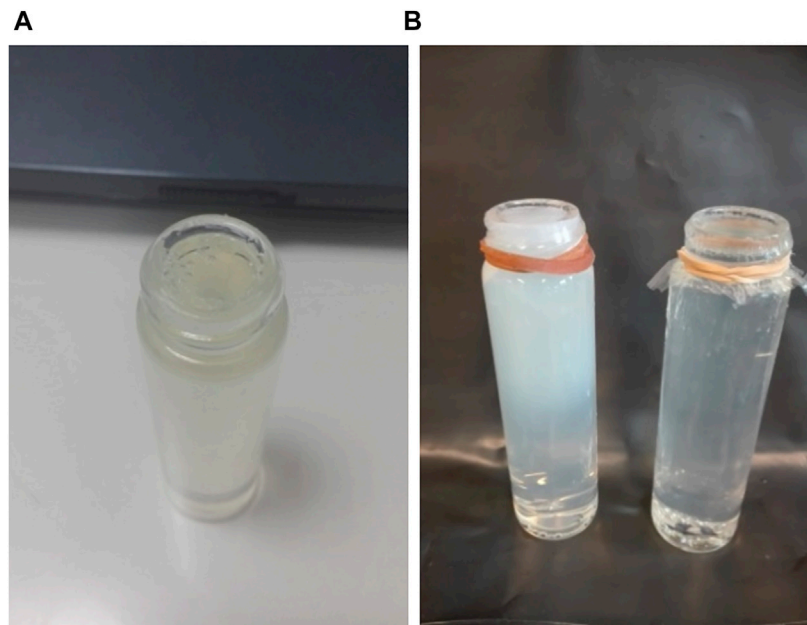


FIGURE 4 | (A) A 2.2 cm diameter, 25 ml small vial container filled with polymer gel. A thin plastic membrane is used on the top of the vial to protect the gel surface. **(B)** An irradiated (white colour) and a non-irradiated gel vial.

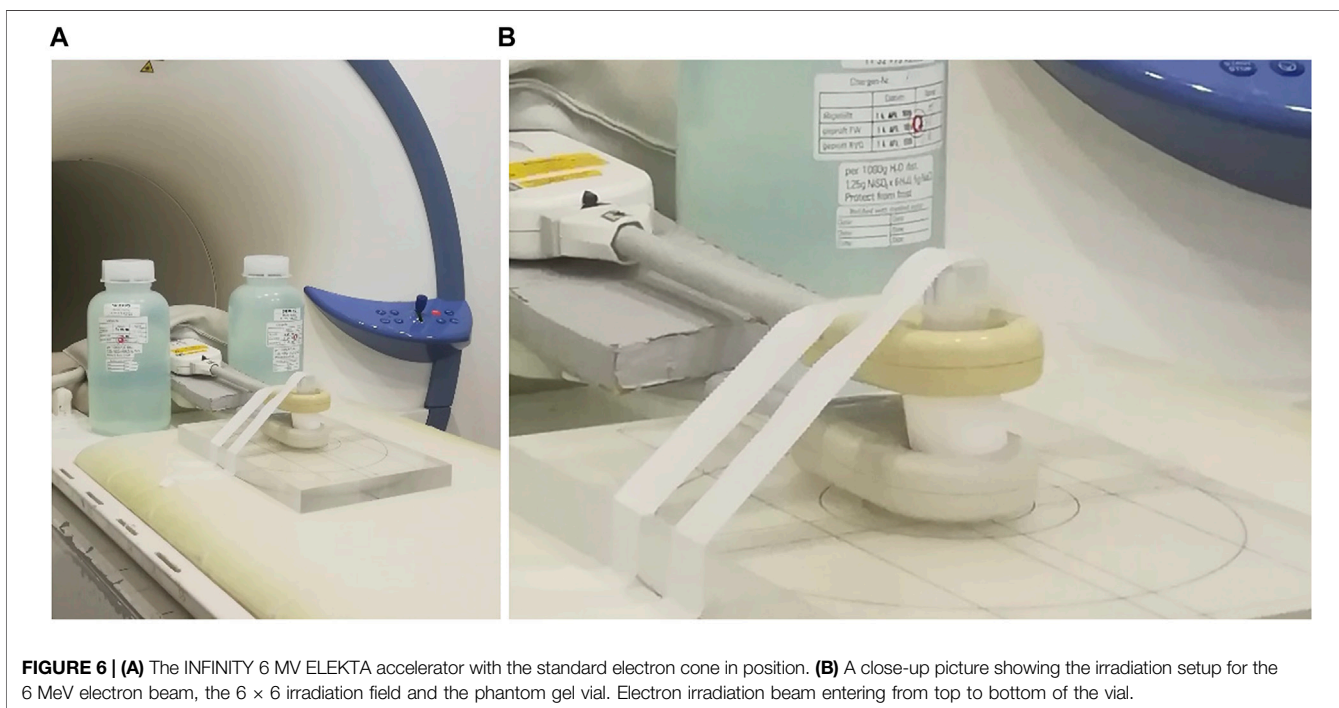
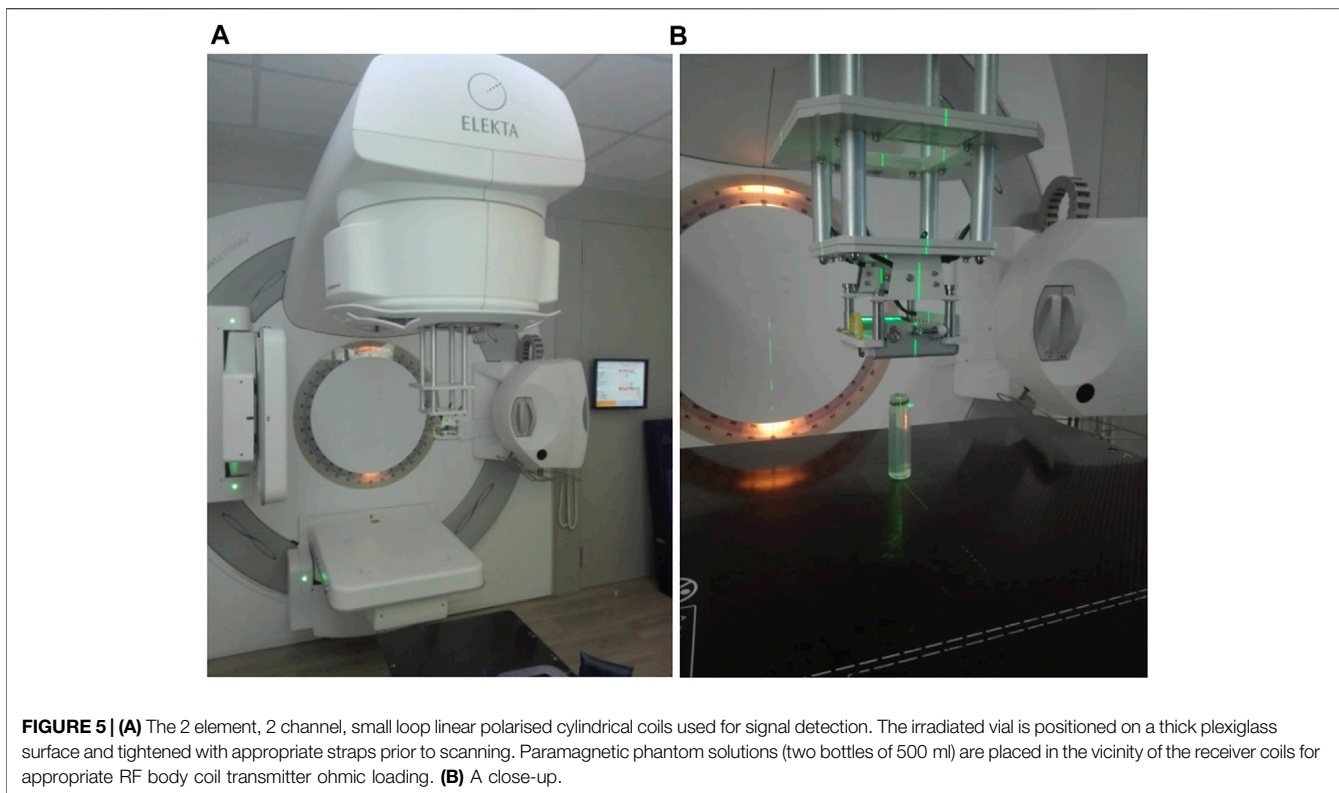
time: 200 μ s, Gradient Slew Rate: 200 (mT/m/ms). A standard quadrature radio frequency (RF) body coil is used in all measurements for signal excitation and a 2 element, 2 channel small diameter (2 cm) linear polarized cylindrical coil is used for signal detection (Figure 6). Each vial is transferred to the isocenter of the magnet and a comprehensive scan protocol is performed. The small vial phantom is placed in supine position (test tubes facing up) and is positioned on the patient layer using the “head first” configuration. A conventional Gradient Echo (GRE) 2D multi slice multi plane turbo Fast Low Angle Shot (turboFLASH) T1 weighted imaging sequence is initially applied in axial, sagittal and coronal planes for the localization of the phantom test tube.

For the quantitative T2 measurements, a 2D Proton Density (PD) to T2 (PD-T2) weighted multi-slice-multi-Echo Half Fourier Single Shot Turbo Spin Echo (HASTE) sequence is used. HASTE sequences have certain important advantages when compared to standard Multi-Echo-Spin-Echo (MESE) sequences, scanning time being the most important [44]. HASTE is a single shot sequence. All the K-space data are obtained sequentially for each slice or echo on the specified TR, utilizing a linear K-space filling order. In HASTE sequences in each TR, approximately 2/3 of K-space is filled. The rest part of the K-space is computed mathematically. The actual contrast in HASTE sequences depends on the effective TE (The TE present when filling the central K-space line). The echo spacing time (time difference between two adjacent K-space lines) is kept as short as possible. The relative change in TE contrast amongst the K-lines of the K-space is minimal. The effective TE in HASTE sequences, is practically the parameter which characterizes the contrast of whole HASTE MR image. Moreover, the T2 values of the non-irradiated to the irradiated gels cover the range of 700 ms down to 300 ms respectively. This is the ideal range for

obtaining signal and relative contrast in HASTE sequences as are initially designed for the clinical applications.

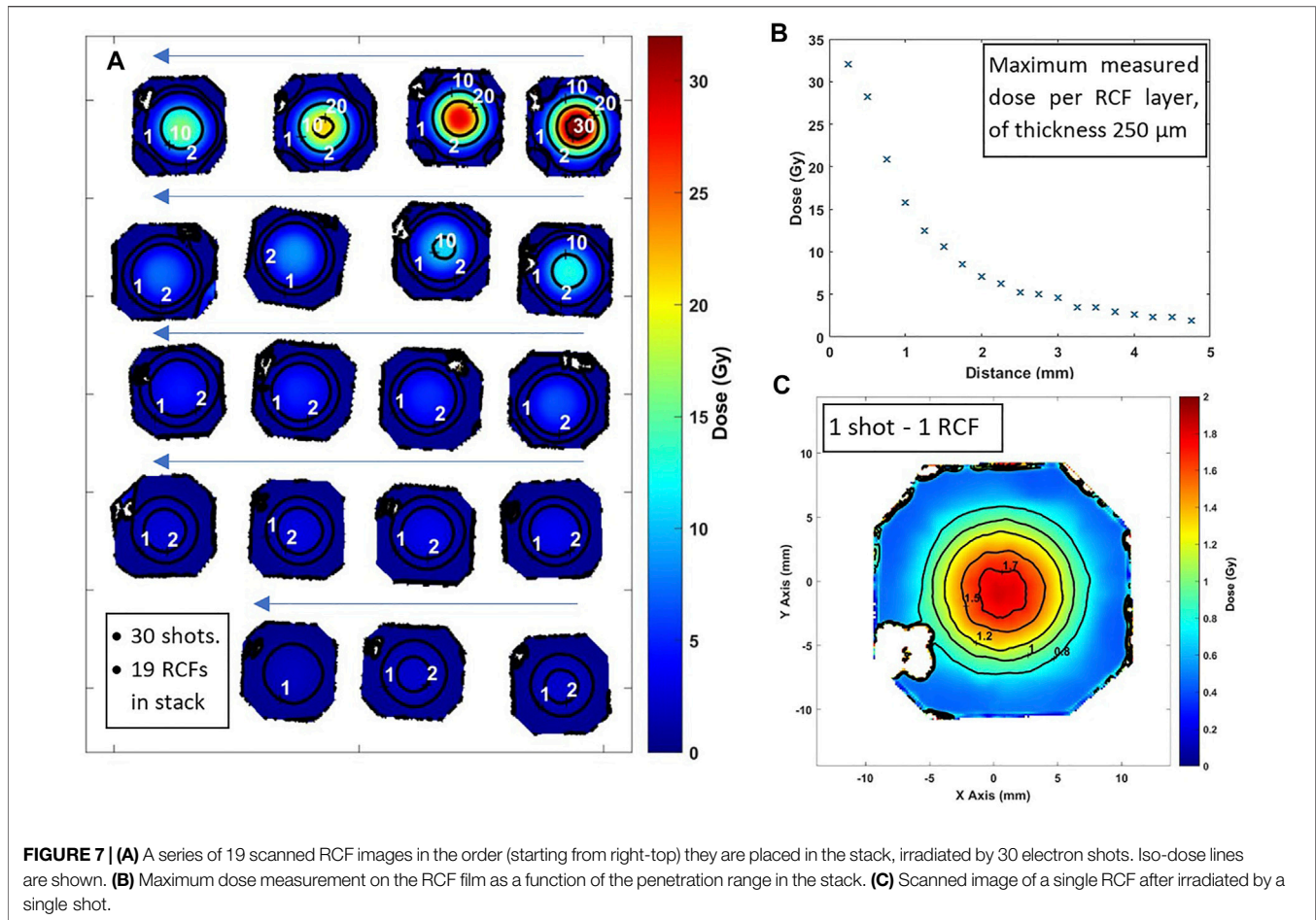
The multi-echo HASTE sequence is applied using four asymmetrically repeated spin echoes. The first echo time (TE) is 61 ms and the rest three TE's are obtained at 606, 1,150 and 1700 ms respectively. A selective refocusing RF pulse scheme is utilized. Thirteen axial (or transverse) space filling slices of 2 mm slice thickness and no interslice gap are used. The longer depicted anatomical axis parallel to the vial's longer dimension (Anterior to Posterior direction for the axial slices) is always chosen as the frequency encoding axis. A repetition time (TR) of 2200 ms and restore magnetization pulse is used in all phantom measurements. A Field Of View (FOV) image area of $35 \times 70 \text{ mm}^2$ is covered from each 2 mm slice. The image reconstruction matrix consists of 128×256 pixels arranged to the FOV such, that a square pixel size of $0,27 \text{ mm} \times 0,27 \text{ mm}$ at slice thickness of 2 mm is obtained. The cross-plane spatial resolution is equal to the slice thickness (2 mm). The overall spatial resolution expressed in data voxel dimension is $0,27 \times 0,27 \times 2 \text{ mm}^3$. The total imaging dimension on the cross-plane direction (all slices and gaps) is 26 mm (13 slices of 2 mm slice thickness) covering the central area of the longitudinal axes of the test tubes.

The highest possible receiver bandwidth (300 Hz/pixel) is used in order to eliminate geometric distortions due to susceptibility artifacts and also to minimize chemical shift artifacts. 2D geometric distortion compensation is also applied in order to eliminate geometric distortions due to inherent gradient field imperfections. The overall signal to noise ratio (SNR) measured on the first echo proton density weighted image of the HASTE sequence is approximately 140 in all phantom experiments. Echo Train Length (ETL) factor is 128 and 32 signal averages are used. The total examination time is approximately 15 min for each vial.



In multi-echo HASTE sequences, an overall long T₂ (300–700 ms) MR signal decaying is assumed along the measured echoes. In MRI gel dosimetry this decay follows a single exponential behaviour. The actual parametric fitting is

performed by utilizing a weighted linear analysis fit on the semi-log decaying MR signal data on a voxel by voxel basis [45]. In the weighted linear fitting method, all the signal intensities are weighted prior to the standard linear fit on all



logarithmic echo signal intensities of the T2 relaxation decay data [45]. The T2 relaxation decay curves are analysed assuming a mono-exponential decay behaviour in the presence of the image stack background which is subtracted from the actual signal data. Each echo signal is corrected via a specific weighting factor prior to the actual weighted linear fit for the final T2 calculation [45].

The final voxel by voxel T2 colour parametric map serves as an indirect measurement of the delivered dose on the gel matrix in 3D. The parametric map image voxel with dimensions $(0.27 \times 0.27 \times 2) \text{ mm}^3$ serves as the minimal measurement volume of the actual 3D gel dosimeter. The T2 measured colour range is presented in the colours of the NIH palette for a range of approximately 500 up to 700 ms. Shorter T2's appear blue and higher T2's appear red in the NIH palette. In relation, higher delivered doses appear blue and lower doses appear red.

3 RESULTS

3.1 Conventional Diagnostics Results

3.1.1 CR39 Results

The CR39 filtered by different thickness of Al layers in 8 sectors is used to determine the proton energies range emitted by the interaction of 1 J laser pulses with the 30 μm thick Al targets.

The energy of the laser generated protons is determined by the known penetration range of protons in aluminium (**Figure 2B**). In particular, the 8-sector filtered CR39 is irradiated by 10 consecutive shots. Following the CR39 etching procedure signal recorded only on the first two sectors the maximum proton energy is evaluated and found to be in the range of 1.5–1.9 MeV [29]. Protons of such energy could not propagate through the 150 μm thick plastic window of the re-entrant tube and therefore the protons do not contribute to the dose deposited in the gel dosimetry.

3.1.2 RCF Diagnostic Results

A stack of 19 RCFs covered by 13 μm Al foil is placed inside the re-entrant tube at a distance of 4 cm from the rear of the target, to measure the electron dose in 30 sequential laser shots onto 30 μm thick Al targets. As mentioned previously, the generated protons cannot pass into the re-entrant tube while the electrons could pass through and contribute to the dose deposited to the RCFs stack. Also, the relative low contribution from photons could be neglected as mentioned in **Section 2.2.2**. The results of the scanned RCFs of the stack are shown in **Figure 7A**. The dose as a function of penetrated distance is shown in **Figure 7B**. In **Figure 7C** a scanned RCF film irradiated by a single electron pulse (one laser shot) is presented. An electron beam with an approximately gaussian profile having less than 10 mm diameter at FWHM is measured and

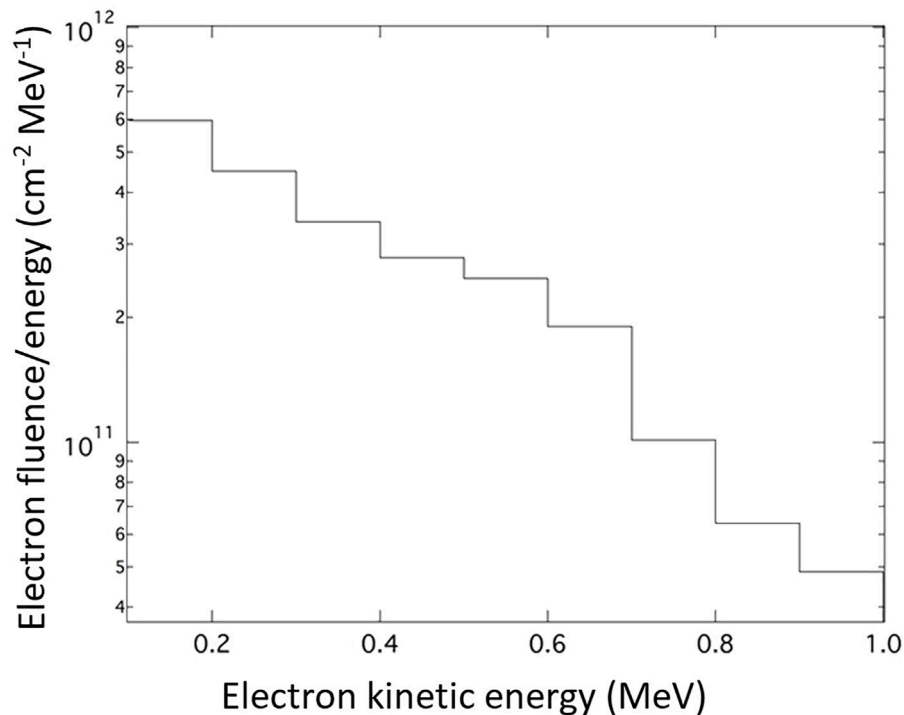


FIGURE 8 | The unfolded electron spectrum in the range between 0.1–1 MeV in the direction along the rear target normal.

the dose is 1.7 Gy at the centre of the beam. From the RCF stack, the spectrum of the electron beam is evaluated following the procedure presented in our previous work [29] and is illustrated in **Figure 8**. Electrons of energy less than 100 keV are stopped by the 13 μm Al foil filter placed in front of the stack. The resulting spectrum shows that the vast majority of the electrons are within the energy window between 0.1 and 1 MeV. Within this energy window the electron spectrum intensity is seen to be decreased by a factor of 10 for the higher energies.

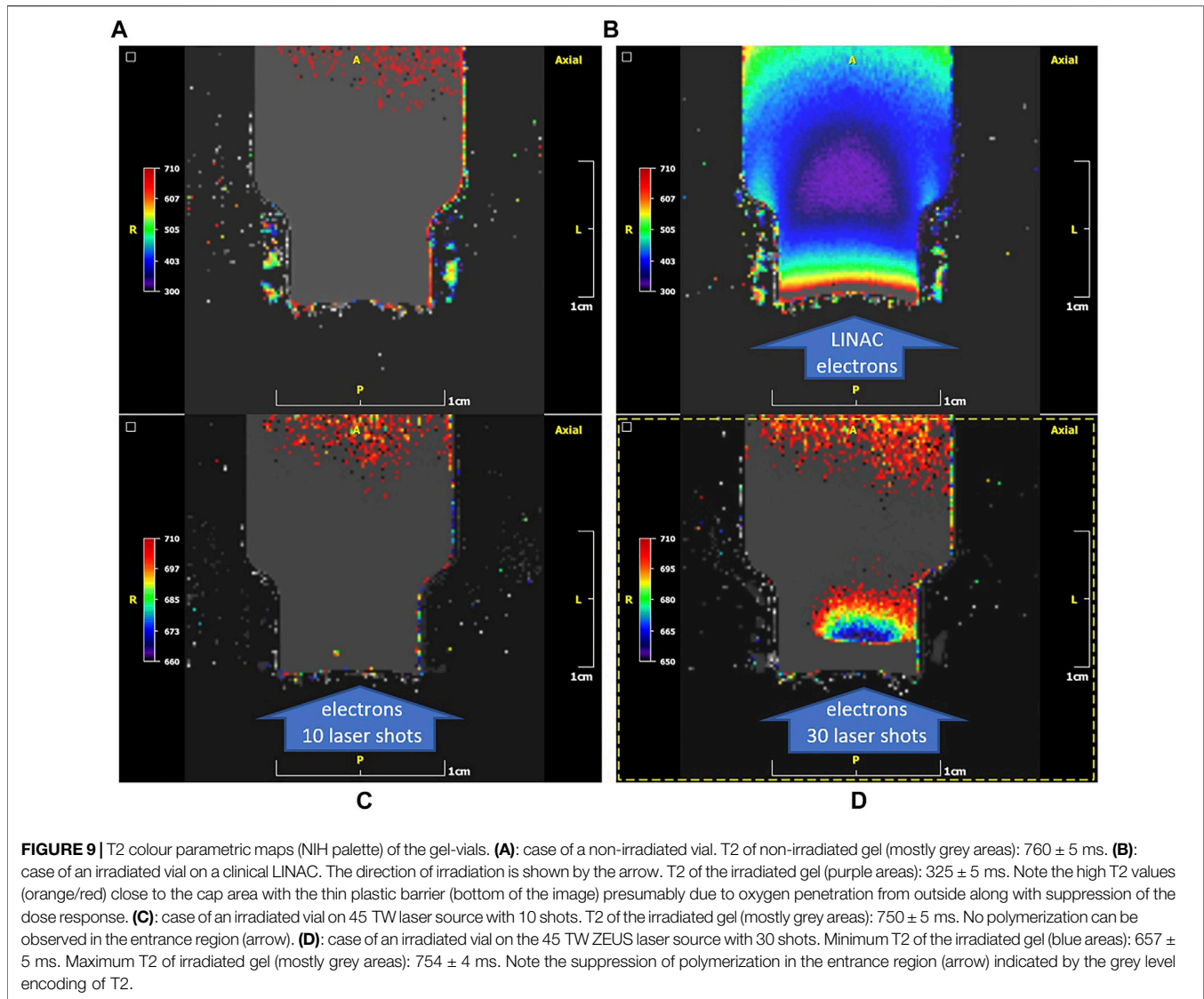
3.2 RESULTS OF POLYMER GEL DOSIMETRY

The polymer gel vials, after their irradiation are stored at 20°C inside a temperature-controlled box for about 24 h and then transferred for MRI evaluation. **Figure 9** presents results of different irradiation cases. In **Figure 9A** the T2 colour parametric map of a non-irradiated vial is presented. T2 is expressed in (ms) utilizing an NIH palette range of 300–710 ms. The T2 of non-irradiated gel (mostly grey areas) is 760 \pm 5 ms. In **Figure 9B** the T2 colour parametric map of an irradiated vial utilizing a clinical LINAC is presented. The T2 is expressed in (ms) utilizing an NIH palette range of 300–710 ms. The region with highest dose features a T2 of 325 \pm 5 ms. In **Figure 9C** the T2 colour parametric map of an irradiated vial on the 45 TW LASER source with 10 shots is presented. The T2 is expressed in (ms) utilizing a NIH palette range of 650–710 ms. The T2 of the irradiated gel (mostly grey areas) is 750 \pm 5 ms. In **Figure 9D**

the T2 colour parametric map of an irradiated vial on a 45 TW laser source with 30 shots is presented. The T2 is expressed in (ms) utilizing the NIH palette range of 650–710 ms. The minimum T2 of the irradiated gel (blue areas) is 657 \pm 5 ms. The maximum T2 of the irradiated gel (mostly grey areas) is 754 \pm 4 ms.

In **Figure 10A** the T2 colour parametric map of the vial irradiated from the open side (“top to bottom”) by 30 shots of the 45 TW laser driven electrons is presented. T2 is expressed in (ms) utilizing the NIH palette range of 500–700 ms. The T2 of the irradiated gel (mean grey/red areas) is 696 \pm 13 ms. Due to suspected influence of oxygen on the gel sensitivity, a “bottom to top” irradiation of the vial is performed by the same number of shots and the T2 colour parametric map is presented in **Figure 10B**. The T2 is expressed in (ms) utilizing the NIH palette range of 500–700 ms. The minimum T2 of the irradiated gel (blue/green areas) is 583 \pm 5 ms. The maximum T2 of irradiated gel (mostly red areas) is 654 \pm 5 ms.

In **Figure 11A** the T2 parametric map of a “bottom to top” configuration vial irradiated with 30 shots of the 45 TW laser driven electrons is presented. T2 is expressed in (ms) utilizing the NIH grey scale palette range of 500–700 ms. In **Figure 11B** the T2 values longitudinal profile for a 2 cm length beginning from the bottom of the vial is presented. In **Figure 11C** the T2 values of a lateral profile for a 1.8 cm length across the vial and for a 1 mm depth from the bottom of the vial is presented. The T2 value is reduced to the half into 3 mm inside the gel (longitudinally) as shown in **Figure 11B**, while from **Figure 11C** a FWHM of 8 mm



for the T2 value in the lateral direction, close to the bottom of the vial, is measured.

4 DISCUSSION

In this study, polymer gel dosimetry based on VIPET polymer gels is utilised for the first time, to characterize the FLASH dose from the electron beam generated by the high intensity laser pulses of the 45 TW ZEUS laser system focused on solid targets. The electron source is generated by the interaction of the of 1 J, 25 fs laser pulses, focused on 30 μm thick Al foils. Using a re-entrant tube, the gel vial is placed under atmospheric pressure at a distance of 4 cm (entrance edge of vials) from the target (source). The conventional CR39 nuclear track detectors are utilised as tool for the analysis of proton depth and energy, accompanied by radiochromic film (RCF) to diagnose the spot, energy range and dose of the secondary electron beam source. The results show that the maximum proton energy is

slightly less than 2 MeV. Protons of such energy cannot propagate through the 150 μm thick plastic window of the re-entrant tube and are therefore eliminated in line with the required experimental parameters. The RCF analysis evaluates an average maximum electron FLASH radiation dose of 1.1 Gy per shot at the centre of the electron beam (**Figure 7A**) while a maximum dose of 1.7 Gy per shot is recorded in some shots (**Figure 7C**).

This initial irradiation study shows that 10 shots of laser generated electrons are not sufficient to polymerize the VIPET gels (**Figure 9C**). As it is found, the use of the thin plastic membrane to protect the gel surface is proven “a critical drawback” in our experiments. The area close to the surface is not sufficiently protected from suppression of the dose response mediated by oxygen diffusion from surrounding atmospheric conditions due to the thin foil barrier. The use of oxygen scavenger THPC in a concentration of 7 mM is not sufficient to protect the sensitive gel from the polymerization due to the existence of the atmospheric oxygen. The presence of the atmospheric oxygen

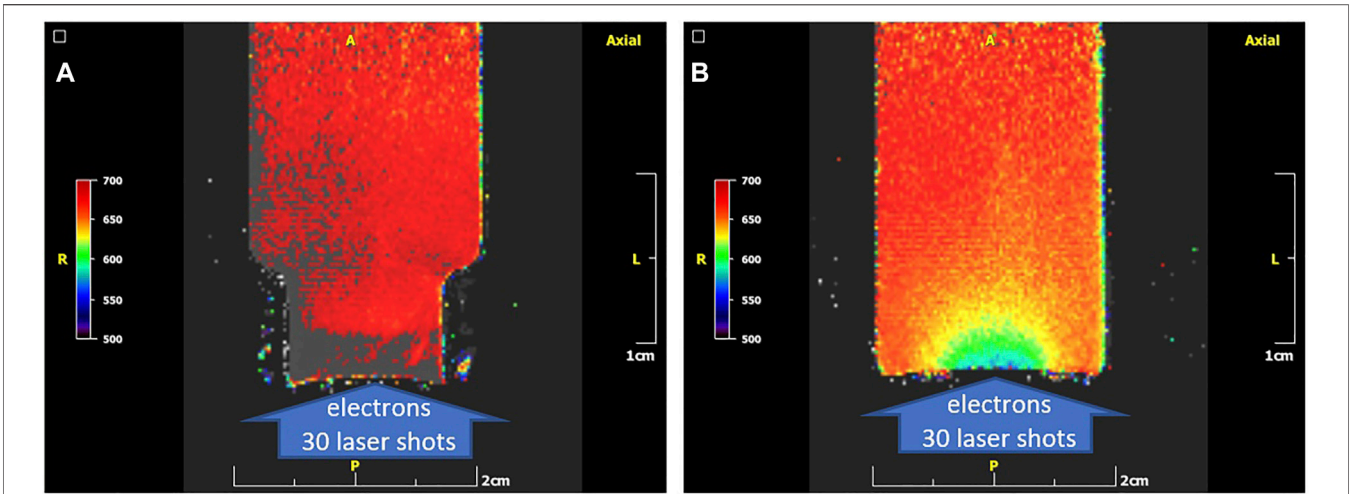


FIGURE 10 | The T2 colour parametric maps (NIH palette) of the gel-vials **(A)**: T2 colour parametric map of a “top to bottom” irradiated vial on a 45 TW laser source with 30 shots. Here the colour scale is adjusted to be the same with that of the “bottom to top” case in the right for direct comparison. T2 of the irradiated gel (mean grey/red areas): 696 ± 13 ms. **(B)**: T2 colour parametric map of “bottom to top” irradiated vial on a 45 TW ZEUS laser source with 30 shots. Minimum T2 of the irradiated gel (blue/green areas): 583 ± 5 ms. Maximum T2 of irradiated gel (mostly red areas): 654 ± 5 ms. The difference in the images **(A,B)** denotes a suppression of dose response in the electron entrance region in the “top to bottom” arrangement most likely due to oxygen penetrating the thin foil there.

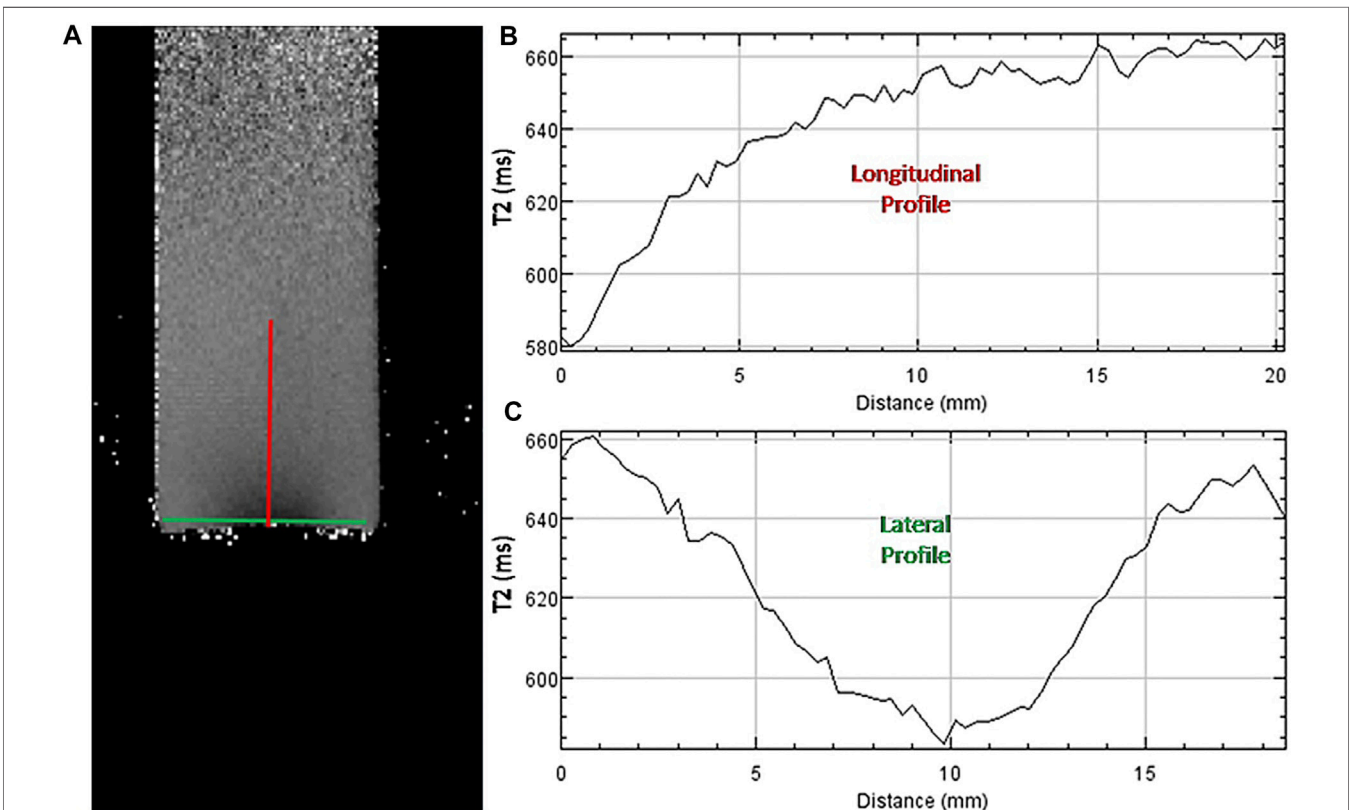


FIGURE 11 | (A): T2 parametric map of the “bottom to top” irradiated vial of **Figure 11B** in greyscale NIH palette range: 500–700 ms. **(B)**: T2 values (ms) longitudinal profile for a 2 cm length along the red line in panel A. **(C)**: T2 values (ms) lateral profile for a 1.8 cm length along the green line in panel A.

reduces the sensitivity of the gel and therefore its polymerization by the electron beam (**Figure 9C**). By increasing the total fluence of the electrons (30 laser shots) the effect of radiation induced polymerization of the gel is clear, although the afore mentioned oxygen-effect obviously affects the result (**Figure 9D**). The same oxygen-effect issue is also present during the irradiation of the vial under a clinical LINAC electron beam (**Figure 9B**). In this case, although the electron energy is also relatively low the total electron fluence is tremendous. This is the reason that the electrons seem to bypass the initial oxygen affected gel layer and deliver their doses at a depth of 1.5 cm from the top of the vial, while they should deposit their energy immediately after their interactions with the gel's molecules.

The oxygen-effect problem is verified in a rather unorthodox way. Instead of irradiating the vials from “top-to-bottom” direction, the irradiation was arranged differently in the reference experiment at a “bottom-to-top” direction. In the standard “top-to-bottom” setup, a layer of the surface entrance is enriched by oxygen penetrating the thin protected membrane and no polymerization occurs (**Figure 10A**). In the reverse setup, at a “bottom-to-top” orientation, oxygen cannot penetrate the thick glass layer of the container. This practically means that during irradiation all the electrons should initially interact with the glass housing of the bottom of the vial (~1.4 mm thick) and then advance to the polymer gel detector. In accordance with the CSDA range in glass for the electron energy spectrum of this study, an amount of ~85% is absorbed, and the residual higher energy electrons pass through the glass material and interact with the gel (**Figure 10B**). The measured changes in the gel due to the irradiation from the laser generated electrons are extended longitudinally into up to 1.5 cm deep inside the gel at the centre of the electron beam (**Figure 11B**). Lateral changes in polymer gel dose response are extending about 7 mm around the beam axis (**Figure 11C**). However, the indicated dose profile is affected by the non-uniform glass bottom of the vial. Although the total electron fluence is relatively low compared with that from LINAC, the gel diagnostic could detect it and provide the ability to characterize the laser generated electron beam.

In conclusion, we present a proof of principle qualitative study on polymer-gel radiation dosimetry of laser-based ultrafast relativistic electron radiation sources. The results demonstrate that polymer gels are in principle capable to offer 3D information on the dose distribution of laser generated electron beams dose and open new research challenges for quantitative analysis. The dependence of the polymer gel response to the extremely high dose rates of electrons irradiation needs to be investigated thoroughly. Technical challenges include studies on the use gel-container of thin homogenous glass bottom to avoid oxygen presence, while minimizing distortion of the electron beam to be measured, as well as on the ability to use the diagnostic into vacuum. Furthermore, the effect of the laser generated FLASH type of the sub-ps duration electron irradiation doses on tissues is itself an open field of research [46]. Differences are expected in radiation biology when comparing the extremely high FLASH dose rates to the relatively continuously applied LINAC dose levels at significantly less dose rates.

In addition, ongoing research includes the use of the gel-radiation dosimetry for electron beams with energies approaching the 100 MeV range, routinely generated by the

interaction of the ZEUS laser pulses with gas jet targets [6, 29]. Furthermore, the tissue to gel phantom material dosimetry equivalency offers unique capabilities for the biomedical applications campaign being developed at the IPPL with the use of the ZEUS laser facility.

DATA AVAILABILITY STATEMENT

The raw data supporting the conclusion of this article will be made available by the authors, without undue reservation.

AUTHOR CONTRIBUTIONS

MT, NAP, TGM and ETD shared the initial project idea and organized the campaign. IF had the main responsibility for writing up this manuscript and was responsible for the ZEUS laser operation during the experiments and the development of optical designs for the experiments. ELC and IF directed the experiments with the ZEUS laser which were contacted with the PhD students AG, ITa, SP and GA. EPB, EB and VD provided key support for the design of the experiment and the development of simulation modelling of the laser generated particle sources. TGM led the gel synthesis, irradiation by LINAC, MRI configuration gel measurements and analysis protocols. Gel synthesis, MRI measurements and analysis were performed by ITs, TB, GK, GB and DAL. EP and ETD provided key support in the interpretation of the gel irradiation results. ELC and TGM wrote the first draft report for the ZEUS experiments and gel dosimetric results respectively. MT, TGM, and NAP reviewed the paper. MT was the scientific coordinator of the funding projects reported below.

FUNDING

This work was conducted within the project “Strengthening the competitiveness of the Region of Crete in cutting-edge medical applications using secondary plasma sources from ultra-strong lasers,” funded by national resources of the Public Investment Program of the Region of Crete (KA-2017EP40200006 of SAEP402). We also acknowledge support by the project “ELI—LASERLAB Europe Synergy, HiPER and IPERION-CH.gr” (MIS 5002735) which is implemented under the Action “Reinforcement of the Research and Innovation Infrastructure”, funded by the Operational Programme “Competitiveness, Entrepreneurship and Innovation” (NSRF 2014–2020) and co-financed by Greece and the European Union (European Regional Development Fund).

ACKNOWLEDGMENTS

We thank Prof. Pantelis Karaiskos and Dr. Ioannis Kantemiris from National and Kapodistrian University of Athens for the fruitful discussion and assistance in this work. We thank the PhD student Aggeliki Doulis and the postgraduate student Simos Vlachos for their contribution to this work.

REFERENCES

- Strickland D, Mourou G. Compression of Amplified Chirped Optical Pulses. *Opt Commun* (1985) 56:219–21. doi:10.1016/0030-4018(85)90120-8
- Tatarakis M, Davies JR, Lee P, Norreys PA, Kassapakis NG, Beg FN, et al. Plasma Formation on the Front and Rear of Plastic Targets Due to High-Intensity Laser-Generated Fast Electrons. *Phys Rev Lett* (1998) 81:999–1002. doi:10.1103/PhysRevLett.81.999
- Clark EL, Krushelnick K, Davies JR, Zepf M, Tatarakis M, Beg FN, et al. Measurements of Energetic Proton Transport through Magnetized Plasma from Intense Laser Interactions with Solids. *Phys Rev Lett* (2000) 84:670–3. doi:10.1103/PhysRevLett.84.670
- Hegelich BM, Albright BJ, Cobble J, Flippo K, Letzring S, Paffett M, et al. Laser Acceleration of Quasi-Monoenergetic MeV Ion Beams. *Nature* (2006) 439:441–4. doi:10.1038/nature04400
- Andrianaki G, Grigoriadis A, Benis EP, Papadogiannis NA. (2020). “Pointing Characteristics of X-Rays Generated by Relativistic Electron Acceleration via 45 TW Fs Laser-He Plasma¹.” In The 22nd International Conference on Ultrafast Phenomena 2020 (OSA Technical Digest), paper Tu4A.12. doi:10.1364/up.2020.tu4a.12
- Grigoriadis A, Andrianaki G, Tatarakis M, Benis EP, Papadogiannis NA. Betatron-type Laser-Plasma X-ray Sources Generated in Multi-Electron Gas Targets. *Appl Phys Lett* (2021) 118:131110. doi:10.1063/5.0046184
- Mangles SPD, Murphy CD, Najmudin Z, Thomas AGR, Collier JL, Dangor AE, et al. Monoenergetic Beams of Relativistic Electrons from Intense Laser-Plasma Interactions. *Nature* (2004) 431:535–8. doi:10.1038/nature02939
- Salamin Y, Hu S, Hatsagortsyan K, Keitel C. Relativistic High-Power Laser-Matter Interactions. *Phys Rep* (2006) 427:41–155. doi:10.1016/j.physrep.2006.01.002
- Esarey E, Schroeder CB, Leemans WP. Physics of Laser-Driven Plasma-Based Electron Accelerators. *Rev Mod Phys* (2009) 81:1229–85. doi:10.1103/RevModPhys.81.1229
- Dromey B, Zepf M, Gopal A, Lancaster K, Wei MS, Krushelnick K, et al. High Harmonic Generation in the Relativistic Limit. *Nat Phys* (2006) 2:456–9. doi:10.1038/nphys338
- Faure J, Glinec Y, Pukhov A, Kiselev S, Gordienko S, Lefebvre E, et al. A Laser-Plasma Accelerator Producing Monoenergetic Electron Beams. *Nature* (2004) 431:541–4. doi:10.1038/nature02963
- Malka V, Faure J, Gauduel YA, Lefebvre E, Rousse A, Phuoc KT. Principles and Applications of Compact Laser-Plasma Accelerators. *Nat Phys* (2008) 4:447–53. doi:10.1038/nphys966
- Wilks SC, Langdon AB, Cowan TE, Roth M, Singh M, Hatchett S, et al. Energetic Proton Generation in Ultra-intense Laser-Solid Interactions. *Phys Plasmas* (2001) 8:542–9. doi:10.1063/1.1333697
- Pukhov A, Meyer-ter-Vehn J. Laser Wake Field Acceleration: the Highly Non-linear Broken-Wave Regime. *Appl Phys B: Lasers Opt* (2002) 74:355–61. doi:10.1007/s003400200795
- Kostyukov I, Nerush E, Pukhov A, Seredov V. A Multidimensional Theory for Electron Trapping by a Plasma Wake Generated in the Bubble Regime. *New J Phys* (2010) 12:045009. doi:10.1088/1367-2630/12/4/045009
- Leemans WP, Gonsalves AJ, Mao H-S, Nakamura K, Benedetti C, Schroeder CB, et al. Multi-GeV Electron Beams from Capillary-Discharge-Guided Subpetawatt Laser Pulses in the Self-Trapping Regime. *Phys Rev Lett* (2014) 113:245002. doi:10.1103/PhysRevLett.113.245002
- Senje L, Coughlan M, Jung D, Taylor M, Nersisyan G, Riley D, et al. Experimental Investigation of Picosecond Dynamics Following Interactions between Laser Accelerated Protons and Water. *Appl Phys Lett* (2017) 110:104102. doi:10.1063/1.4977846
- Chaudhary P, Milluzzo G, Ahmed H, Odlozilik B, McMurray A, Prise KM, et al. Radiobiology Experiments with Ultra-high Dose Rate Laser-Driven Protons: Methodology and State-Of-The-Art. *Front Phys* (2021) 9:75. doi:10.3389/fphy.2021.624963
- Kurup A, Pasternak J, Taylor R, Murgatroyd L, Ettliger O, Shields W, et al. Simulation of a Radiobiology Facility for the Centre for the Clinical Application of Particles. *Physica Med* (2019) 65:21–8. doi:10.1016/j.ejmp.2019.07.003
- Bolton PR, Borghesi M, Brenner C, Carroll DC, De Martinis C, Fiorini F, et al. Instrumentation for Diagnostics and Control of Laser-Accelerated Proton (Ion) Beams. *Physica Med* (2014) 30:255–70. doi:10.1016/j.ejmp.2013.09.002
- Downer MC, Zgadaj R, Debus A, Schramm U, Kaluza MC. Diagnostics for Plasma-Based Electron Accelerators. *Rev Mod Phys* (2018) 90:035002. doi:10.1103/RevModPhys.90.035002
- Bisesto F, Galletti M, Anania MP, Ferrario M, Pompili R, Botton M, et al. Review on TNSA Diagnostics and Recent Developments at SPARC_LAB. *High Pow Laser Sci Eng* (2019) 7:e56. doi:10.1017/hpl.2019.41
- Galimberti M, Giulietti A, Giulietti D, Gizzi LA. SHEEBA: A Spatial High Energy Electron Beam Analyzer. *Rev Scientific Instr* (2005) 76:053303. doi:10.1063/1.1899309
- Pianoschi T, Alva-Sánchez M, Santanna M, César D, Nicolucci P. SU-E-T-278: Study of MAGIC-F Gel and PENELOPE Code Simulation Response for Clinical Electron Beams. *Med Phys* (2012) 39:3767. doi:10.1118/1.4735346
- Liu H, Li J, Pappas E, Andrews D, Evans J, Werner-Wasik M, et al. Dosimetric Validation for an Automatic Brain Metastases Planning Software Using Single-Isocenter Dynamic Conformal Arcs. *J Appl Clin Med Phys* (2016) 17:142–56. doi:10.1120/jacmp.v17i5.6320
- Hillbrand M, Landry G, Ebert S, Dedes G, Pappas E, Kalaitzakis G, et al. Gel Dosimetry for Three Dimensional Proton Range Measurements in Anthropomorphic Geometries. *Z für Medizinische Physik* (2019) 29:162–72. doi:10.1016/j.zemedi.2018.08.002
- Pappas E, Kalaitzakis G, Boursianis T, Zoros E, Zourari K, Pappas EP, et al. Dosimetric Performance of the Elekta Unity MR-Linac System: 2D and 3D Dosimetry in Anthropomorphic Inhomogeneous Geometry. *Phys Med Biol* (2019) 64:225009. doi:10.1088/1361-6560/ab52ce
- Trapp JV, Partridge M, Hansen VN, Childs P, Bedford J, Warrington AP, et al. The Use of Gel Dosimetry for Verification of Electron and Photon Treatment Plans in Carcinoma of the Scalp. *Phys Med Biol* (2004) 49:1625–35. doi:10.1088/0031-9155/49/9/003
- Clark EL, Grigoriadis A, Petrakis S, Tazes I, Andrianaki G, Skoulakis A, et al. High-intensity Laser-Driven Secondary Radiation Sources Using the ZEUS 45 TW Laser System at the Institute of Plasma Physics and Lasers of the Hellenic Mediterranean University Research Centre. *High Pow Laser Sci Eng* (2021) 9:e53. doi:10.1017/hpl.2021.38
- Palmer AL, Dimitriadis A, Nisbet A, Clark CH. Evaluation of Gafchromic EBT-XD Film, with Comparison to EBT3 Film, and Application in High Dose Radiotherapy Verification. *Phys Med Biol* (2015) 60:8741–52. doi:10.1088/0031-9155/60/22/8741
- Groza A, Chiroasca A, Stancu E, Butoi B, Serbanescu M, Dregheci DB, et al. Assessment of Angular Spectral Distributions of Laser Accelerated Particles for Simulation of Radiation Dose Map in Target Normal Sheath Acceleration Regime of High Power Laser-Thin Solid Target Interaction-Comparison with Experiments. *Appl Sci* (2020) 10:4390. doi:10.3390/APP10124390
- Sipilä P, Ojala J, Kajaluoto S, Jokelainen I, Kosunen A. Gafchromic EBT3 Film Dosimetry in Electron Beams - Energy Dependence and Improved Film Read-Out. *J Appl Clin Med Phys* (2016) 17:360–73. doi:10.1120/jacmp.v17i1.5970
- Gorbics SG, Pereira NR. Differential Absorption Spectrometer for Pulsed Bremsstrahlung. *Rev Scientific Instr* (1993) 64:1835–40. doi:10.1063/1.1144019
- Baldock C, De Deene Y, Doran S, Ibbott G, Jirasek A, Lepage M, et al. Polymer Gel Dosimetry. *Phys Med Biol* (2010) 55:R1–R63. doi:10.1088/0031-9155/55/5/R01
- Bloembergen N, Purcell EM, Pound RV. Relaxation Effects in Nuclear Magnetic Resonance Absorption. *Phys Rev* (1948) 73:679–712. doi:10.1103/PhysRev.73.679
- Gustavsson H, Bäck SÅJ, Medin J, Grusell E, Olsson LE. Linear Energy Transfer Dependence of a Normoxic Polymer Gel Dosimeter Investigated Using Proton Beam Absorbed Dose Measurements. *Phys Med Biol* (2004) 49:3847–55. doi:10.1088/0031-9155/49/17/002
- Schreiner LJ, Olding T, McAuley KB. Polymer Gel Dosimetry. *J Phys Conf Ser* (2010) 250:012014. doi:10.1088/1742-6596/250/1/012014
- Deene YD. Fundamentals of MRI Measurements for Gel Dosimetry. *J Phys Conf Ser* (2004) 3:87–114. doi:10.1088/1742-6596/3/1/009
- Pappas E, Maris T, Angelopoulos A, Pappargiopolou M, Sakelliou L, Sandilos P, et al. A New Polymer Gel for Magnetic Resonance Imaging (MRI) Radiation Dosimetry. *Phys Med Biol* (1999) 44:2677–84. doi:10.1088/0031-9155/44/10/320

40. Papadakis AE, Maris TG, Zacharopoulou F, Pappas E, Zacharakis G, Damilakis J. An Evaluation of the Dosimetric Performance Characteristics of N-Vinylpyrrolidone-Based Polymer Gels. *Phys Med Biol* (2007) 52:5069–83. doi:10.1088/0031-9155/52/16/024
41. Maryanski MJ, Gore JC, Kennan RP, Schulz RJ. NMR Relaxation Enhancement in Gels Polymerized and Cross-Linked by Ionizing Radiation: a New Approach to 3D Dosimetry by MRI. *Magn Reson Imaging* (1993) 11:253–8. doi:10.1016/0730-725X(93)90030-H
42. Baldock C, Burford RP, Billingham N, Wagner GS, Patval S, Badawi RD, et al. Experimental Procedure for the Manufacture and Calibration of Polyacrylamide Gel (PAG) for Magnetic Resonance Imaging (MRI) Radiation Dosimetry. *Phys Med Biol* (1998) 43:695–702. doi:10.1088/0031-9155/43/3/019
43. Hepworth SJ, Leach MO, Doran SJ, Berger CM, Byers JD, Henderson CL, et al. Dynamics of Polymerization in Polyacrylamide Gel (PAG) Dosimeters: (II) Modelling Oxygen Diffusion. *Phys Med Biol* (1999) 44:1875–84. doi:10.1088/0031-9155/44/8/302
44. Maris TG, Pappas E, Boursianis T, Kalaitzakis G, Papanikolaou N, Watts L, et al. 3D Polymer Gel MRI Dosimetry Using a 2D Haste, A 2D TSE and A 2D SE Multi echo (ME) T2 Relaxometric Sequences: Comparison of Dosimetric Results. *Physica Med* (2016) 32:238–9. doi:10.1016/j.ejmp.2016.07.498
45. Kalaitzakis GI, Papadaki E, Kavroulakis E, Boursianis T, Marias K, Maris TG. Optimising T2 Relaxation Measurements on MS Patients Utilising a Multi-Component Tissue Mimicking Phantom and Different Fitting Algorithms in T2 Calculations. *Hell J Of Radiol* (2019) 4:18–31. doi:10.36162/hjr.v4i2.293
46. Labate L, Palla D, Panetta D, Avella F, Baffigi F, Brandi F, et al. Toward an Effective Use of Laser-Driven Very High Energy Electrons for Radiotherapy: Feasibility Assessment of Multi-Field and Intensity Modulation Irradiation Schemes. *Sci Rep* (2020) 10:17307. doi:10.1038/s41598-020-74256-w

Conflict of Interest: The authors declare that the research was conducted in the absence of any commercial or financial relationships that could be construed as a potential conflict of interest.

Publisher's Note: All claims expressed in this article are solely those of the authors and do not necessarily represent those of their affiliated organizations, or those of the publisher, the editors and the reviewers. Any product that may be evaluated in this article, or claim that may be made by its manufacturer, is not guaranteed or endorsed by the publisher.

Copyright © 2022 Fitis, Grigoriadis, Tazes, Petrakis, Andrianaki, Dimitriou, Bakarezos, Benis, Tsiapa, Boursianis, Kalaitzakis, Bontzos, Liakopoulos, Pappas, Detorakis, Clark, Maris, Papadogiannis and Tatarakis. This is an open-access article distributed under the terms of the Creative Commons Attribution License (CC BY). The use, distribution or reproduction in other forums is permitted, provided the original author(s) and the copyright owner(s) are credited and that the original publication in this journal is cited, in accordance with accepted academic practice. No use, distribution or reproduction is permitted which does not comply with these terms.